Plasma Physics Reports, Vol. 31, No. 10, 2005, pp. 871–885. Translated from Fizika Plazmy, Vol. 31, No. 10, 2005, pp. 939–953.

LOW-TEMPERATURE PLASMA

Study of the Dark Phase in the Initial Stage of the Positive Column Formation in an Argon Glow Discharge

N. A. Dyatko[1], Yu. Z. Ionikh[2], A. V. Meshchanov[2], and A. P. Napartovich[1]

[1] *Troitsk Institute for Innovation and Thermonuclear Research, Troitsk, Moscow oblast, 142090 Russia*

[2] *Fock Research Institute of Physics, St. Petersburg State University, Ul'yanovskaya ul. 1, Petrodvorets, St. Petersburg, 198504 Russia*

Received November 18, 2004; in final form, December 27, 2004

Abstract—The initial stage of the positive column formation in an argon glow discharge is investigated both experimentally and theoretically. A decrease in the plasma radiation intensity (the so-called "dark phase") was observed experimentally over a time period of about 1 ms. A similar dip was also observed in the time dependence of the electric field strength. The time evolution of the population of the lowest metastable state of Ar was measured. A relevant theoretical model has been developed and used to perform calculations for the actual experimental conditions. A comparison between the numerical and experimental results shows that the model adequately describes the processes that occur during the formation of the positive column in an argon glow discharge. Experimental and theoretical study shows that the dark-phase effect is related to an excessive amount of metastable Ar atoms at the beginning of a discharge and, consequently, to high rates of stepwise ionization and chemionization. *© 2005 Pleiades Publishing, Inc.*

1. INTRODUCTION

The so-called "dark phase" in the initial stage of the positive column formation was first observed in [1, 2], where glow discharges in pure helium and its mixtures with small additives of nitrogen or carbon oxide were investigated under conditions such that the time intervals between the discharge pulses were fairly long. It was found that, when the output voltage of the power supply was high enough, i.e., when the discharge current was mainly determined by the ballast resistance rather than the resistance of the discharge itself, the discharge displayed a number of specific features. In particular, after a short and very intense emission peak at the beginning of the current pulse, the emission intensity from all the spectral lines and bands dropped and remained almost zero over a certain period of time. The dark phase (DP) lasted from a few tens of microseconds to a few milliseconds. The emission intensity then rapidly increased and reached a steady-state level (generally, after a few oscillations). In this case, the discharge current, which was controlled by the ballast resistance, remained almost constant throughout the discharge pulse. A similar effect was observed in a continuous discharge after additional excitation of the plasma by a high-voltage nanosecond pulse [3, 4].

In [2], this effect was explained as follows: In discharges excited in mixtures of helium with a small additive of a molecular gas M, the main ionization process is Penning ionization,

$$\mathrm{He^*} + \mathrm{M} \longrightarrow \mathrm{He} + \mathrm{M^+} + e. \qquad (1)$$

At the beginning of the discharge, when the discharge current is low, the discharge voltage is high and the electric field in the discharge is much higher than its steady-state value. This results in the intense excitation of the gas atoms and molecules and the generation of the initial spike in the emission intensity. At the same time, an excessive amount of metastable atoms are produced. As a consequence, after the current has reached its steady-state level, the density of the electrons produced in reaction (1) is much higher than that in the steady-state phase of the discharge. This leads to a redistribution of the voltage between the discharge and the ballast resistance, the electric field in the discharge decreasing below its steady-state value, and the excitation rate becoming very low. Since the rate of ambipolar diffusion under these conditions is also low, the excess electrons very slowly escape to the wall, so the DP duration can significantly exceed the decay time of the metastable atoms.

In pure helium, reaction (1) does not occur; in this case, however, its role can be played by the two-body collision reaction between metastable He atoms,

$$\mathrm{He^*} + \mathrm{He^*} \longrightarrow \mathrm{He^+} + \mathrm{He} + e. \qquad (2)$$

Processes similar to reaction (2) take place in other noble gases as well. Therefore, it is reasonable to expect that the DP effect will also manifest itself in them. The aim of this study was to observe and study the DP effect in argon.

2. EXPERIMENTAL SETUP

The experimental setup was similar to that described in [2]. The diameter of the U-shaped discharge tube made of molybdenum glass was 2.7 cm, the length of

1063-780X/05/3110-0871$26.00

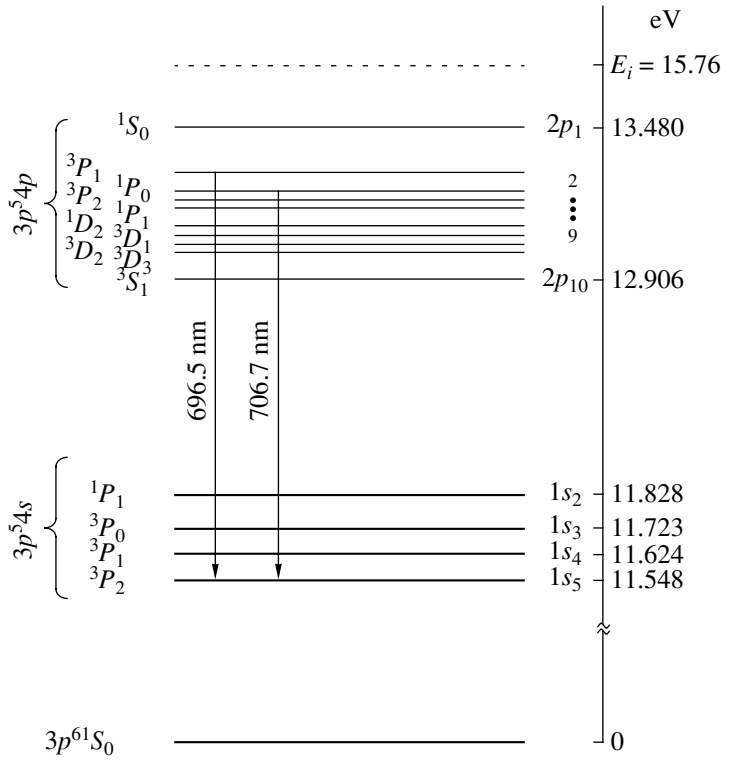

Fig. 1. Schematic diagram of the lower electronic states of Ar.

its horizontal part was 12 cm, and the distance between the cylindrical Ti electrodes was 30 cm. The anode was grounded. Spectrally pure argon (99.999%) was continuously pumped through the discharge tube and a system of liquid-nitrogen traps. A repetitive discharge was produced by means of an electronic switch set in parallel to the discharge tube. The response time of the switch was 0.3 μs.

Optical measurements were performed along the axis of the horizontal part of the tube. The plasma radiation was recorded using a monochromator with a 1200-line/mm diffraction grating, an FEU-106 photomultiplier operating in the photon counting regime, a pulsed amplifier, a 256-channel reverse photon counter with a time resolution of 1 μs (designed by G.V. Zhuvikin and V.A. Ivanov), and a PC. The concentration of metastable Ar atoms was determined from the absorption of the probing radiation produced by a small-size hollow cathode and propagating along the axis of the discharge tube. The ratio between the widths of the emission and absorption lines was found by the method described in [2]. We also measured the integral (over wavelengths) emission intensity from different points of the positive column. These measurements were performed across the tube using a movable photomultiplier tube.

The electric field in the plasma was determined using probes set at the discharge axis, 2.7 cm from one another. The probe signals were fed to a digital oscilloscope through a high-resistance divider and differential amplifier.

3. EXPERIMENTAL RESULTS

Figure 1 shows a schematic diagram of the lower electronic states of Ar. The arrows show the spectral lines whose emission intensities were measured in our experiments.

By analyzing the time evolution of the emission intensity from the positive column, we determined the experimental conditions at which the DP effect was present in an argon discharge. It was found that the pressure should be a few torr and the discharge current should be about 1 mA. Moreover, as was said above, the output voltage of the power supply and the ballast resistance must be high enough. Most of the experiments were carried out at a pressure of $p = 5$ torr, steady-state current of $i = 0.7$ mA, supply voltage of $U = 3.6$ kV, and ballast resistance of $R_b = 4.45$ MΩ. Under these conditions, the reduced electric field was $E/N = 5.5$ Td (when calculating the atomic density N, the gas temperature was assumed to be 300 K, which is the upper estimate found from the heat conduction equation). The corresponding electron density averaged over the discharge cross section was $\sim 1.5 \times 10^9$ cm^{-3}.

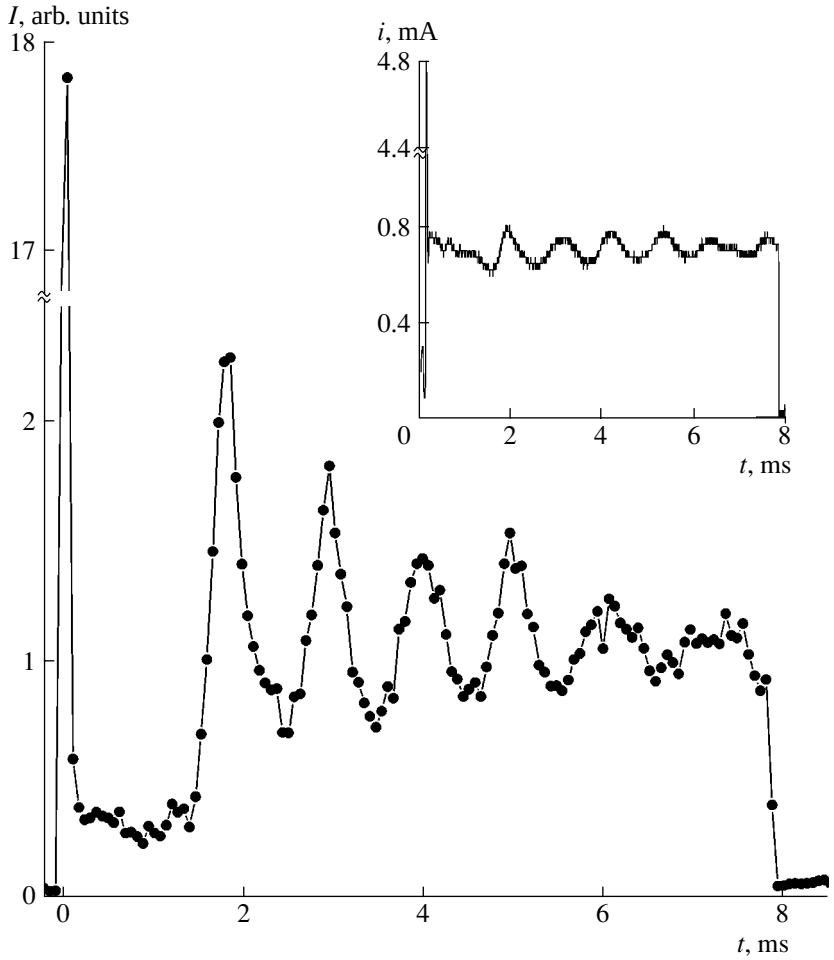

Fig. 2. Measured time evolution of the emission intensity of the 696.5-nm line for $p = 5$ torr, $i = 0.7$ mA, and $T = 80$ ms. The insert shows the waveform of the discharge current.

Figure 2 shows the measured time evolution of the intensity of the Ar 696.5-nm line for a discharge duration of $\tau = 8$ ms and repetition period of $T = 80$ ms. In fact, this is a single-pulse mode because the time interval between pulses is much longer than the plasma decay time (the electron density decreases by two orders of magnitude over a time of $T-\tau = 72$ ms). The line intensity shows a sharp spike at the instant of discharge ignition, and then, over a time interval of about 1.5 ms, it is much lower than that in the steady-state phase. After this, it sharply increases again, performs several oscillations, and reaches a steady-state level. Similar behavior of the plasma radiation intensity was observed in helium [1, 2]; however, the emission intensity of helium plasma during the DP was two orders of magnitude lower than that in the steady-state phase, whereas, in the case of argon, it was only four times lower. The intensities of the other Ar spectral lines behaved in the same manner.

In argon, the range of discharge currents at which the DP was observed was much narrower than that in helium and its mixtures. As the current increased above 1 mA, the effect became less pronounced. This can be seen from Fig. 3, which corresponds to a current of 1.4 mA ($R_b = 2.2$ MΩ). In this case, the emission intensity during the DP was only two times lower than that in the steady state phase. At higher discharge currents, the DP disappeared. This also occurred when the time interval between the discharge pulses was reduced (Fig. 4). In this case, the initial spike in the emission intensity also disappeared. Such behavior is similar to that observed in helium [1, 2].

Figure 5 shows the measured time evolution of the reduced electric field for the conditions corresponding to Figs. 2–4. It can be seen that the time behavior of E/N correlates with that of the line emission intensities. In a single-pulse operating mode (Figs. 5a, 5e; $T = 80$ ms), the reduced field E/N shows a spike at the instant of discharge ignition, a nearly zero value during the DP, and oscillations in the rest of the discharge. Note that the sharp change in the discharge voltage and the low electron density just after breakdown did not allow us to

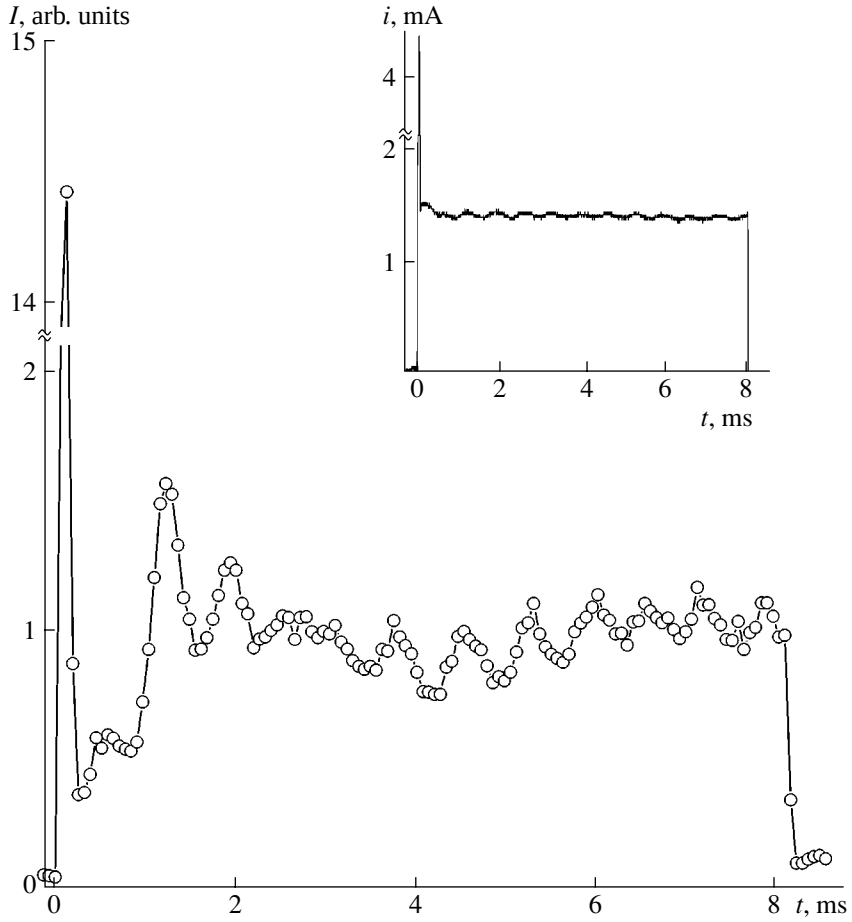

Fig. 3. Measured time evolution of the emission intensity of the 706.7-nm line for $p = 5$ torr, $i = 1.4$ mA, and $T = 80$ ms. The insert shows the waveform of the discharge current.

correctly measure the electric field in the initial stage of the discharge (as well as just after discharge termination). Nevertheless, the electric field during the DP is certainly much lower than the steady-state field. As the time interval between the pulses decreased, the time dependences of the reduced electric field became smoother (see Figs. 5b, 5c) and, then, both the initial spike and the subsequent dip disappeared.

After discharge ignition, the concentration of the $1s_5$ metastable Ar atoms becomes four to ten times higher than that in the steady-state phase (Figs. 6, 7). During the DP, their concentration decreases twofold as compared to that in the steady-state phase. The characteristic decay time of metastable levels during the DP is appreciably shorter than that after the end of the discharge (cf. Figs. 6a, 6b, 7a, and 7b). This can be explained by the large density of the electrons and $Ar(1s_5)$ atoms and, accordingly, the large quenching rate of these levels (see Section 5). A decrease in the time interval between the discharge pulses leads to a substantial decrease in the amplitude of the initial spike in the concentration of metastable atoms.

All the time dependences shown in Figs. 2–7 display oscillations with a period of about 1 ms. Oscillations in the electric field and the local emission intensity (measured across the discharge) were also observed in continuous discharges: at a current of 0.7 mA, the oscillation period was the same as in pulsed discharges, whereas, at a current of 1.4 mA, it was 1.5 times shorter. Optical measurements performed across a continuous discharge showed that the oscillation phase depended monotonically on the photomultiplier position; this means that these oscillations are related to moving striations. Similar measurements performed in a single-pulse mode ($T = 80$ ms) showed a different picture (Fig. 8). In this case, the phases of optical signals from different points along the discharge axis were the same; therefore, the oscillations were caused by in-phase oscillations of the emission intensity from the positive column as a whole. A significant misphasing of oscillations, indicating the origin of moving striations, was observed only at the end of the discharge.

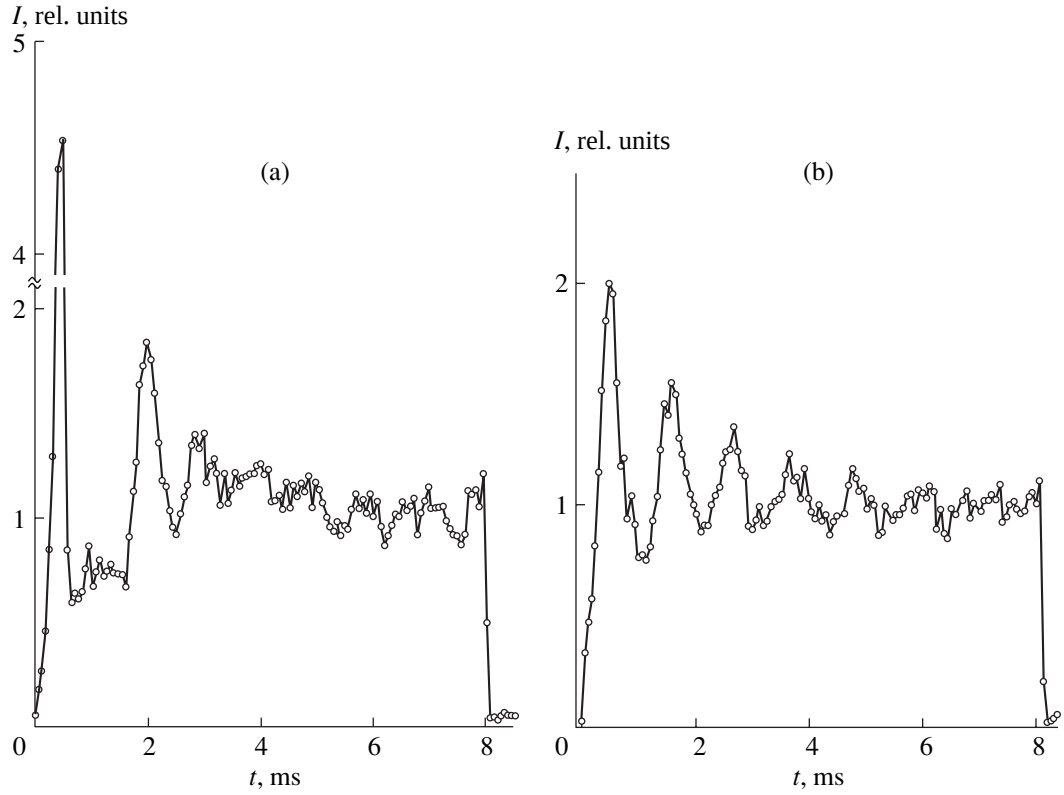

Fig. 4. Measured time evolution of the emission intensity of the 696.5-nm line for $p = 5$ torr, $i = 0.7$ mA, and $T =$ (a) 9 and (b) 8.2 ms.

4. THEORETICAL MODEL

In order to reveal the mechanisms responsible for the DP effect in the positive column of a glow discharge in argon, we have analyzed all the available literature data on the processes governing the population of the excited states and the ionization balance in an argon discharge under actual experimental conditions. Based on these data, a theoretical model has been developed that describes the time evolution of the parameters of the positive column over the time interval from applying the discharge voltage to establishing a steady state. The equations for the electron and ion densities and for the populations of the excited states, the Boltzmann equation for the electron energy distribution function (EEDF), and the equation for the electric circuit are solved self-consistently. The model does not account for the electrode sheaths; i.e., it concerns only the positive column, which is assumed to be uniform along the tube. In other words, the so-called zero-dimensional model is used to describe the kinetics of the electrons, ions, and excited atoms. A schematic of the lower electronic states of Ar is shown in Fig. 1, and the processes included in the model are listed in the table. Let us consider the model in more detail.

The kinetics of the four lower electronic states of Ar is thoroughly taken into account. Two of these levels ($1s_5$ and $1s_3$) are metastable, whereas the other two ($1s_4$ and $1s_2$) are resonant. By analogy to [5], the higher electronic states are combined into two effective levels (F and A), with the level F being the sum of the $3p^5 4p$ levels.

We used the same transport cross section for electron scattering by Ar atoms, cross sections for excitation of electronic levels from the ground state, and cross section for ionization from the ground state as in [5]. In that paper, the rate constants for the excitation of the $1s_5$, $1s_4$, $1s_3$, and $1s_2$ levels were measured and compared to those calculated by solving the Boltzmann equation. The set of cross sections obtained in [5] provides good agreement between the calculated and measured excitation rate constants. Moreover, the calculated values of the drift velocity and the ionization coefficient are also in good agreement with the available experimental data. Therefore, we may consider this set of the cross sections to be self-consistent.

In [5], the transport cross section was chosen according to a recommendation in [6], whereas the ionization cross section was taken from [7]. The values of these cross sections are known with a high accuracy. However, there is a large scatter in both the experimental and theoretical data on the maximum values of the cross sections for the excitation of the $1s_5$, $1s_4$, $1s_3$, and $1s_2$ levels. The maximum of the cross sections for the excitation of the lower $1s_5$ metastable level varies from

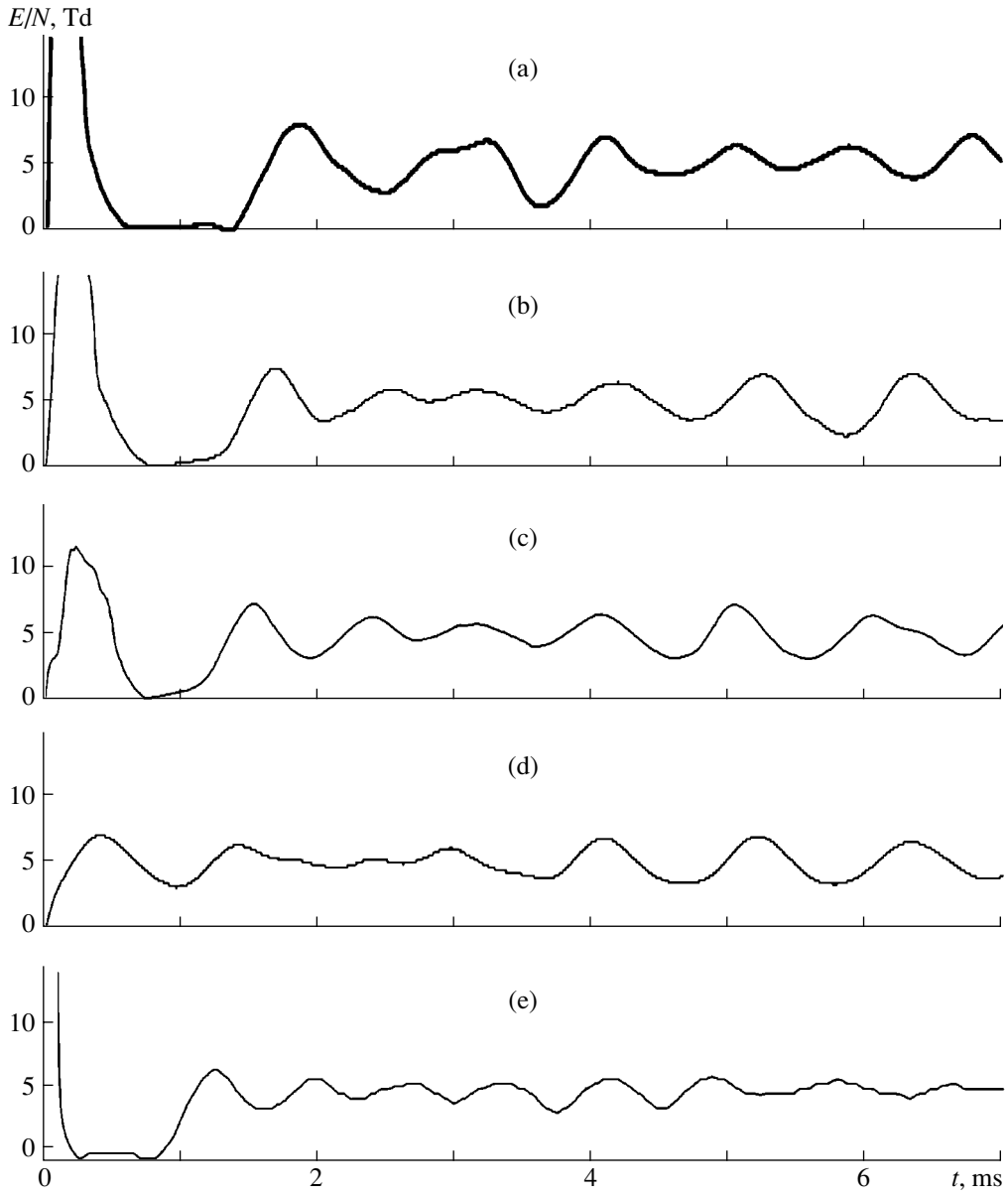

Fig. 5. Measured time evolution of the reduced electric field for p = 5 torr, i = (a–d) 0.7 and (e) 1.4 mA, and T = (a, e) 80, (b) 10, (c) 9, and (d) 8.2 ms.

0.4×10^{-17} cm^2 (experiment [9]) to 10^{-17} cm^2 (experiment [8]) and even to 2.3×10^{-17} cm^2 (computations [8]). There is also scatter in the data on the cross sections for the excitation of the $1s_4$, $1s_3$, and $1s_2$ levels. Note that, in [5], the cross sections for the excitation of the $1s_5$, $1s_4$, $1s_3$, and $1s_2$ levels were taken from [9]; i.e., the minimal known values of these cross sections were used. In this respect, the set of cross sections used in [5] is open to question.

Under our experimental conditions, the main channel for the loss of charged particles is their diffusion to the tube wall. Within the zero-dimensional model of the positive column of a glow discharge, this process is usually characterized by the rate of ambipolar diffusion. When the plasma contains several ion species, the diffusive loss of the charged particles cannot be reduced to conventional ambipolar diffusion only [10]. In our model, we consider two positive ion species: Ar^+ and Ar_2^+. To describe the diffusive loss of the ions and electrons within the zero-dimensional model, we simplified the problem by assuming that the radial profiles of the densities of different ion species are identical and the electron mobility is constant over the tube radius. A general reason for such a simplification is that the mobilities of these ions are close to one another (see

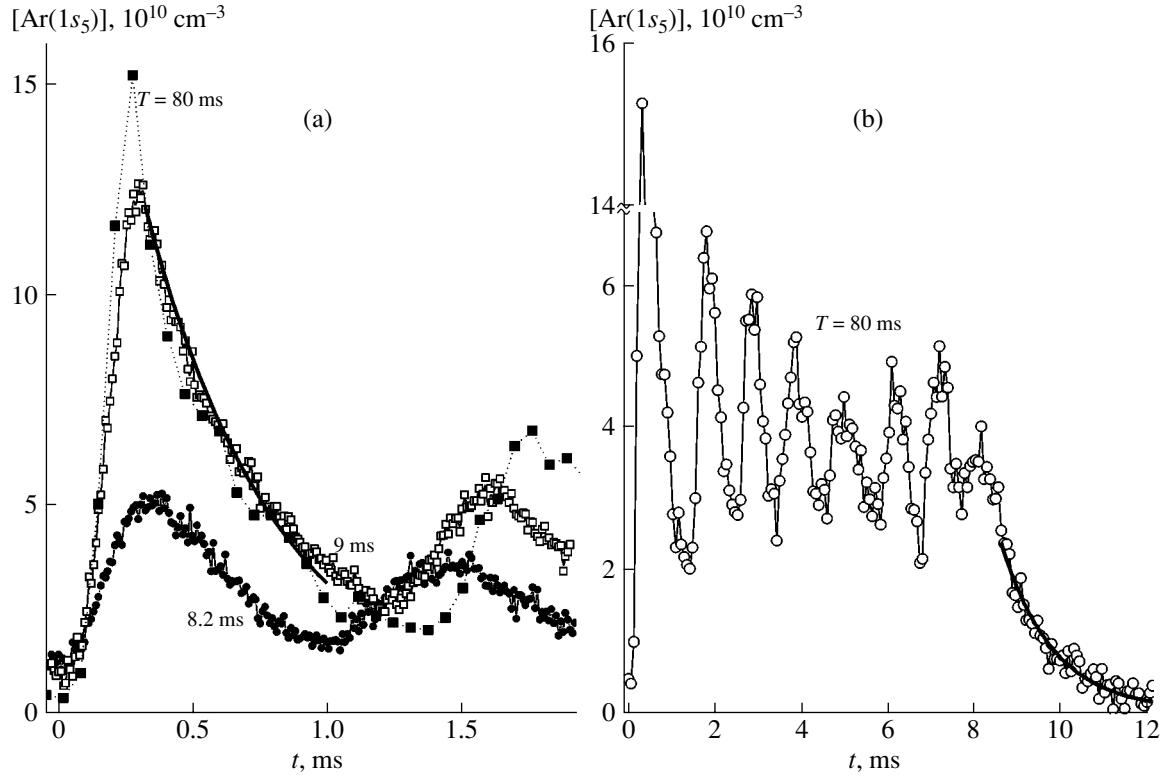

Fig. 6. Measured time evolution of the density of the $1s_5$ metastable Ar atoms (a) in the initial stage of the discharge and (b) throughout the entire discharge for $p = 5$ torr and $i = 0.7$ mA. The heavy solid lines show the exponentials with time constants of (a) 500 μs and (b) 1.2 ms.

below) and the electric field is nearly constant along the tube radius.

In this case, the coefficient of ambipolar diffusion for electron is

$$D_{ea} \approx \frac{D_e}{\mu_e}\left(\frac{n_1}{n_e}\mu_1 + \frac{n_2}{n_e}\mu_2\right), \quad (3)$$

whereas for ions, the coefficients of ambipolar diffusion are

$$D_{1a} \approx \frac{D_e}{\mu_e}\mu_1, \quad D_{2a} \approx \frac{D_e}{\mu_e}\mu_2. \quad (4)$$

In formulas (3) and (4), D_{ea}, D_e, μ_e, and n_e are the coefficient of ambipolar diffusion, the coefficient of free electron diffusion, the electron mobility, and the electron density, respectively; D_{1a}, μ_1, and n_1 are the coefficient of ambipolar diffusion, mobility, and density of Ar^+ ions; and D_{2a}, μ_2, and n_2 are the coefficient of ambipolar diffusion, mobility, and density of Ar_2^+ ions. The plasma is assumed to be quasineutral; i.e., $n_1 + n_2 = n_e$. Formulas (3) and (4) can readily be obtained using a standard procedure for deriving the coefficient of ambipolar diffusion (see, e.g., [11]). The electron mobility and the coefficient of electron diffusion were found by solving the Boltzmann equation for the EEDF. The ion mobilities under normal conditions were taken to be $\mu_1 = 1.6$ cm^2 V^{-1} s^{-1} and $\mu_2 = 2.7$ cm^2 V^{-1} s^{-1} [12].

For a cylindrical discharge tube, the electron diffusion loss rate is equal to

$$\nu_{ea} = \frac{D_{ea}}{\Lambda^2}, \quad (5)$$

$$\Lambda \approx R/2.4, \quad (6)$$

where Λ is the effective diffusion length. Formulas (5) and (6) were obtained from the solution to the Schottky diffusion equation for the electron density [13], in which the ionization term was assumed to be proportional to n_e. This is the case, e.g., when the atoms and molecules are primarily ionized by electron impact from the ground state. In glow discharges in noble gases, stepwise ionization is dominant; i.e., the ionization rate is proportional to n_e^2. Generally speaking, the use of formulas (5) and (6) in this case is unjustified. Nevertheless, it is possible to use formula (5) for the rate of ambipolar diffusion if one redefines the effective diffusion length, as was done in [14, 15]. In particular, it was shown in [15] that, when the ionization rate

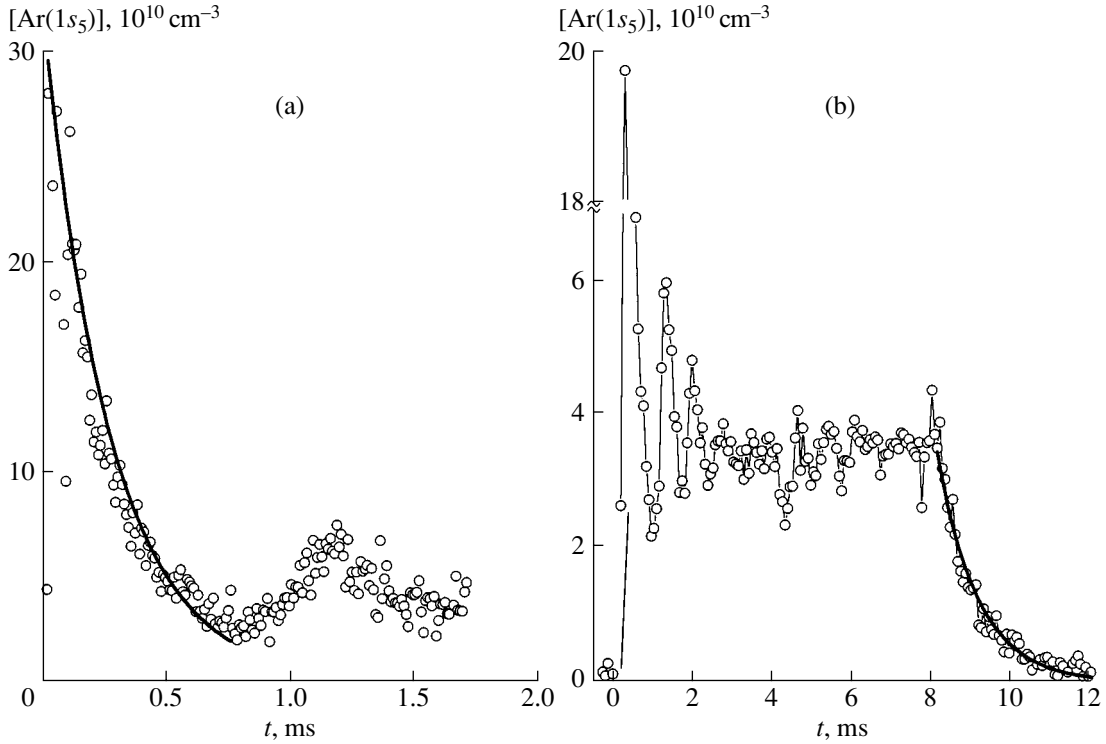

Fig. 7. Measured time evolution of the density of the $1s_5$ metastable Ar atoms (a) in the initial stage of the discharge and (b) throughout the entire discharge for $p = 5$ torr, $i = 1.4$ mA, and $T = 80$ ms. The heavy solid lines show the exponentials with time constants of (a) 270 μs and (b) 1.0 ms.

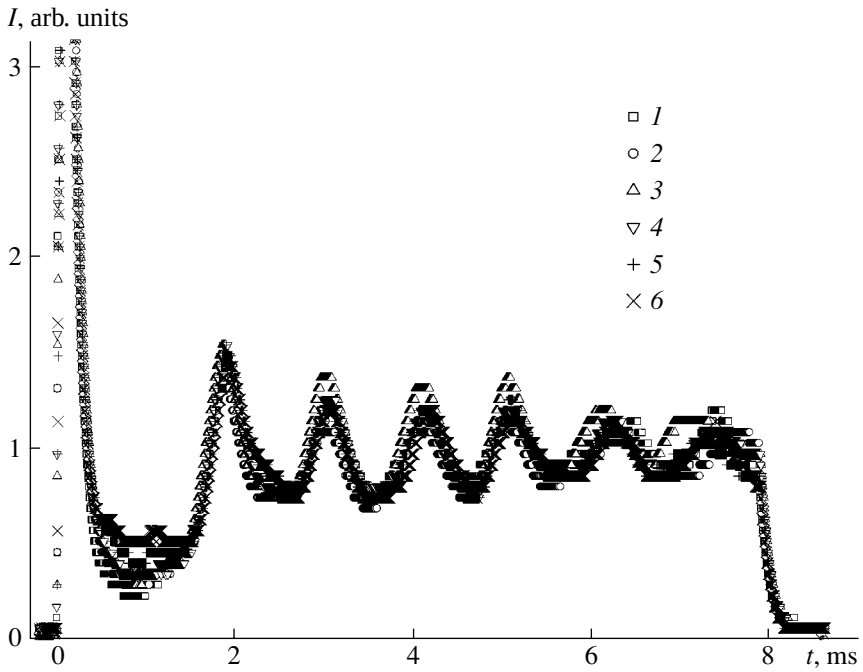

Fig. 8. Integral (over wavelengths) emission intensity measured at different points (*1–6*) spaced a distance of 1 cm from one another along the positive column for $p = 5$ torr, $i = 0.7$ mA, and $T = 80$ ms.

Processes incorporated in the model

No.	Process	k, $cm^6\ s^{-1}$, $cm^3\ s^{-1}$, s^{-1}	References
	Elastic electron scattering		
1	$Ar + e \longrightarrow Ar + e$	Boltzmann equation	[6]
	Excitation from the ground state		
2	$Ar + e \rightleftharpoons Ar(1s_5) + e$	Boltzmann equation	[5]
3	$Ar + e \rightleftharpoons Ar(1s_4) + e$	Boltzmann equation	[5]
4	$Ar + e \rightleftharpoons Ar(1s_3) + e$	Boltzmann equation	[5]
5	$Ar + e \rightleftharpoons Ar(1s_2) + e$	Boltzmann equation	[5]
6	$Ar + e \rightleftharpoons Ar(F) + e$	Boltzmann equation	[5]
7	$Ar + e \rightleftharpoons Ar(A) + e$	Boltzmann equation	[5]
	Ionization from the ground state		
8	$Ar + e \longrightarrow Ar^+ + e + e$	Boltzmann equation	[7]
	Stepwise ionization		
9	$Ar(1s_5) + e \longrightarrow Ar^+ + e + e$	Boltzmann equation	[17]
10	$Ar(1s_3) + e \longrightarrow Ar^+ + e + e$	Boltzmann equation	[17]
	Chemionization		
11	$Ar(1s_5) + Ar(1s_5) \longrightarrow Ar^+ + Ar + e$ $Ar_2^+ + e$	$1.2 \times 10^{-9}\ cm^3\ s^{-1}$	[20, 21]
12	$Ar(1s_3) + Ar(1s_3) \longrightarrow Ar^+ + Ar + e$ $Ar_2^+ + e$	$1.2 \times 10^{-9}\ cm^3\ s^{-1}$	See the text
13	$Ar(1s_5) + Ar(1s_3) \longrightarrow Ar^+ + Ar + e$ $Ar_2^+ + e$	$1.2 \times 10^{-9}\ cm^3\ s^{-1}$	See the text
	Ion conversion		
14	$Ar + Ar^+ + Ar \longrightarrow Ar_2^+ + Ar$	$2.5 \times 10^{-31}\ cm^6\ s^{-1}$	[24]
	Recombination		
15	$Ar_2^+ + e \longrightarrow Ar(A) + Ar$	Boltzmann equation	See the text
	Ambipolar diffusion		
16	$e \longrightarrow$ Tube wall		See the text
17	$Ar_2^+ \longrightarrow$ Tube wall		See the text
18	$Ar^+ \longrightarrow$ Tube wall		See the text
	Electron mixing		
19	$Ar(1s_5) + e \longrightarrow Ar(1s_4) + e$	$2 \times 10^{-7}\ cm^3\ s^{-1}$	See the text
20	$Ar(1s_3) + e \longrightarrow Ar(1s_4) + e$	$2 \times 10^{-7}\ cm^3\ s^{-1}$	See the text
	Emission		
21	$Ar(1s_4) \longrightarrow Ar + h\nu$	$5 \times 10^4\ s^{-1}$	See the text
22	$Ar(1s_2) \longrightarrow Ar + h\nu$	$2.5 \times 10^5\ s^{-1}$	See the text
	Additional electron mixing		
23	$Ar(1s_5,1s_3) + e \longrightarrow Ar(1p_1, \ldots, 1p_{10}) + e$		See the text
24	$Ar(1p_1, \ldots, 1p_{10}) \longrightarrow Ar(1s_2, \ldots, 1s_5) + h\nu$		See the text
	Atomic mixing		
25	$Ar(1s_5) + Ar \longrightarrow Ar(1s_4) + Ar$	$2.3 \times 10^{-15}\ cm^3\ s^{-1}$	[5], See the text
26	$Ar(1s_3) + Ar \longrightarrow Ar(1s_4) + Ar$	$4.3 \times 10^{-15}\ cm^3\ s^{-1}$	[5], See the text
	Formation of dimers		
27	$Ar(1s_5) + Ar + Ar \longrightarrow Ar_2^* + Ar \longrightarrow Ar + Ar + Ar + h\nu$	$1.4 \times 10^{-32}\ cm^6\ s^{-1}$	[5], See the text

Table. (Contd.)

No.	Process	k, $cm^6\ s^{-1}$, $cm^3\ s^{-1}$, s^{-1}	References
28	$Ar(1s_3) + Ar + Ar \longrightarrow Ar_2^* + Ar \longrightarrow Ar + Ar + Ar + h\nu$	$1.5 \times 10^{-32}\ cm^6\ s^{-1}$	[5], See the text
	Diffusion		
29	$Ar(1s_5) \longrightarrow$ Tube wall $\longrightarrow Ar$	$D_0 = 0.09\ cm^2\ s^{-1}$ (under normal conditions)	[5], See the text
30	$Ar(1s_3) \longrightarrow$ Tube wall $\longrightarrow Ar$	$D_0 = 0.09\ cm^2\ s^{-1}$ (under normal conditions)	[5], See the text
	Cascade population		
31	$Ar(A) \longrightarrow Ar(F) + h\nu$		See the text
32	$Ar(F) \longrightarrow Ar(1s_2, \ldots, 1s_5) + h\nu$		See the text

depends quadratically on the electron density, the effective diffusion length can be defined as

$$\Lambda \approx R/1.78. \quad (7)$$

It can easily be seen that the use of expression (7) (instead of (6)) in formula (5) leads to a decrease in the rate of ambipolar diffusion by a factor of 1.8. In our base model, when determining the rate of ambipolar diffusion, the effective diffusion length was calculated by formula (7).

In this context, we should mention paper [16] devoted to the experimental and theoretical study of the steady-state parameters of the positive column of an argon glow discharge. In that paper, in order to fit the simulation results to the measurement data, the rate of ambipolar diffusion was decreased severalfold.

The cross sections for stepwise ionization from the $3p^54s$ levels were taken from measurements [17]. Note that the calculated values of these cross sections [18, 19] agree well with the experimental results of [17]. It is assumed in our model that stepwise ionization occurs only from the $1s_5$ and $1s_3$ metastable levels because the populations of the $1s_4$ and $1s_2$ resonant levels (as well as of the higher electronic levels) are small compared to the population of the $1s_5$ state.

The rate constant for chemionization with the participation of Ar atoms in the $1s_5$ metastable state (see table, process no. 11) was taken from [20, 21]. The rate constants for similar reactions with the participation of Ar atoms in the $1s_3$ state (process nos. 12, 13) were assumed to be the same. The yield of molecular ions in these reactions was assumed to be 5% [22]. It should be noted that, in [16, 23], the chemionization rate constant was taken to be approximately one-half that in [20, 21].

The rate constant for the three-body conversion of Ar^+ ions into Ar_2^+ ions was taken from [24]. The energy dependence of the cross section for the dissociative recombination of electrons with Ar_2^+ molecular ions was assumed to depend on the electron energy u as Cu^{-1}. For such an energy dependence of the cross section and a Maxwellian EEDF, the recombination rate constant depends on the electron temperature T_e as $\alpha_r \sim T_e^{-0.5}$, which agrees with theoretical and experimental data [25]. The normalizing factor C was chosen such that $\alpha_r = 7 \times 10^{-7}\ cm^3/s$ at $T_e = 300$ K [25].

An important channel for quenching metastable Ar states is electron-impact excitation from the $1s_5$ and $1s_3$ states to the $1s_4$ and $1s_2$ resonant states (process nos. 19, 20) with a subsequent radiative transition to the ground state (process nos. 21, 22). The cross sections for process nos. 19 and 20 were calculated in [26, 27] and were then used in [28] to determine the rate constants for these processes as a function of the electron temperature. The calculated total rate constant for the quenching of the $1s_5$ level ($k \approx 8 \times 10^{-8}\ cm^3/s$ at $T_e = 1.5$ eV) turned out to be far less than the measured one ($k \approx 2 \times 10^{-7}\ cm^3/s$ at $T_e = 1$–1.7 eV [29]). An additional channel for the electron-impact mixing of metastable and resonant levels is the excitation of the $3p^54p$ states with subsequent radiative transition to different $3p^54s$ states (process nos. 23, 24). This channel was not considered separately in our model. For process nos. 19 and 20, the mixing rate constant was set at $2 \times 10^{-7}\ cm^3/s$, assuming that this effective value accounts for process nos. 23 and 24. Moreover, using the literature data on the cross sections for stepwise excitation from $3p^54s$ to $3p^54p$ levels [30–33] (process no. 23), we studied the role of these processes in the EEDF formation under actual experimental conditions. It was found that these processes only slightly affect the EEDF, which is obviously related to the low relative population of metastable states (~10^{-6}).

The radiative decay of the $1s_4$ and $1s_2$ resonance states was considered in the effective lifetime approximation [34]: $\tau_{eff}^{-1} = A\theta$, where A is the probability of spontaneous emission and θ is the probability of a photon escaping from the region under study (the trapping

of radiation was thus taken into account). According to [34], in the case of cylindrical symmetry, we have

$$\theta = \frac{1}{4}\sqrt{\frac{\lambda}{2\pi R}},$$

where λ is the radiation wavelength and R is the tube radius. The calculated values of τ_{eff}^{-1} are listed in the table (process nos. 21, 22). The necessary data on the probabilities of spontaneous emission and the radiation wavelengths were taken from [35].

The decay rate of the lower metastable states of Ar as a function of the gas pressure was studied in [5], where the rates were determined for three types of loss of excited atoms: (i) the loss rate is inversely proportional to the atomic density, (ii) the loss rate is proportional to the atomic density, and (iii) the loss rate is proportional to the atomic density squared. The first type corresponds to the diffusive escape of the excited atoms to the tube wall (process nos. 29, 30), the second type is associated with the mixing of the metastable and resonant atomic levels (process nos. 27, 28), and the third type is related to the formation of dimers and their subsequent rapid radiative decay (process nos. 27, 28). The diffusion coefficients and the rate constants for the relevant processes were taken from [5]. Note that the rate constant for the dimer formation presented in the table agrees well with the data from [36]. It should also be noted that, under our experimental conditions, the diffusive loss of metastable atoms is insignificant.

At the very beginning of a discharge, when the electric field in the plasma is high enough, the higher electronic states are mainly excited. Radiative transitions from these states populate the $3p^5 4s$ levels (see, e.g., [16]). To take into account this cascade population, the model incorporates the processes of spontaneous emission (process nos. 31, 32). The characteristic times of these processes are very short. Hence, it was supposed that the cascade population proceeds instantaneously. It is also necessary to know the fractions of the cascade population from the effective level F (which is a combination of the $3p^5 4p$ levels) to each of the four levels of the $3p^5 4s$ state. According to [5], these fractions are 40%, 24%, 7%, and 29% for the $1s_5$, $1s_4$, $1s_3$, and $1s_2$ levels, respectively.

The equation for the electric circuit was written in the form

$$(U - V_c - EL)/R_b = en_e V_d (S/2.3),$$

where U is the applied voltage, E is the electric field in the plasma, V_c is the cathode fall, L is the interelectrode distance, R_b is the ballast resistance, e is the electron charge, V_d is the electron drift velocity, S is the cross-sectional area of the tube, and n_e is the electron density at the tube axis. The factor 2.3 corresponds to the Bessel radial profile of the electron density. The cathode fall was assumed to be time-independent (V_c = 100 V).

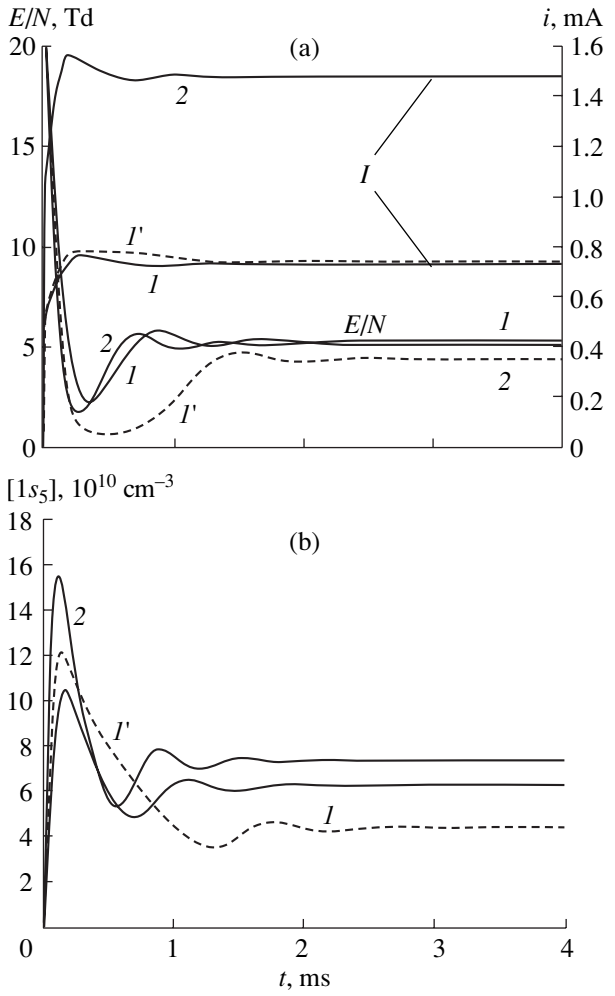

Fig. 9. Calculated time evolution of (a) the discharge current and the reduced electric field in the positive column and (b) the population of the lowest metastable state of Ar for R_b = (*1*) 4.45 and (*2*) 2.2 MΩ. Curves *1*' stand for calculations performed in the test model for R_b = 4.45 MΩ: the cross sections for the excitation of metastable states are increased twofold, the ambipolar diffusion rate is halved, and the rate constant for the mixing of the electronic states by electrons is decreased fourfold.

The Boltzmann equation for the EEDF was solved with allowance for electron–electron collisions and superelastic collisions with excited atoms. The cross sections for superelastic collisions were calculated using the detailed balance principle. The procedure for numerically solving the Boltzmann equation is described in [37]. Note that the EEDF was calculated in the local approximation. The applicability of this approximation under our experimental conditions is disputable. Thus, it was asserted in [38] that the local approximation is inapplicable in argon up to $pR \approx$ 10 cm torr. In our case, $pR \approx 7$ cm torr; therefore, one should expect only qualitative (rather than exact quantitative) agreement between the computation and experimental results.

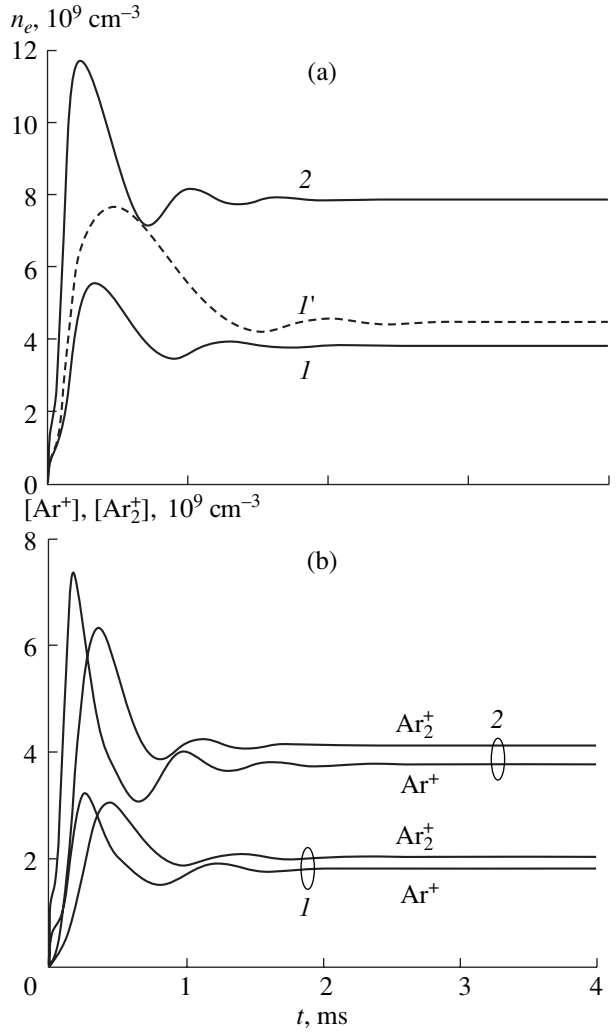

Fig. 10. Calculated time evolution of the (a) electron density and (b) positive ion densities for R_b = (*1*) 4.45 and (*2*) 2.2 MΩ. Curve *1*' stands for calculations performed in the test model for R_b = 4.45 MΩ: the cross sections for the excitation of metastable states are increased twofold, the ambipolar diffusion rate is halved, and the rate constant for the mixing of the electronic states by electrons is decreased fourfold.

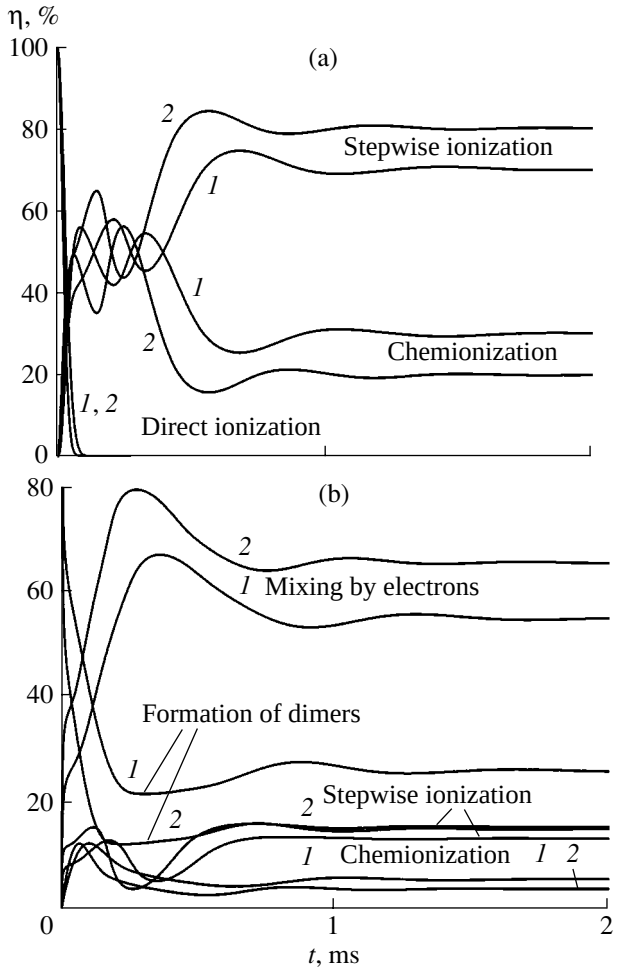

Fig. 11. Calculated time evolution of the relative contributions from different processes to (a) ionization and (b) the decay of the lowest metastable level of Ar for R_b = (*1*) 4.45 and (*2*) 2.2 MΩ.

5. RESULTS OF CALCULATIONS AND COMPARISON TO EXPERIMENT

We performed computations for a pressure of p = 5 torr, supply voltage of U = 3.6 kV, ballast resistance of R_b = 4.45 and 2.225 MΩ, discharge tube length of L = 30 cm, and tube radius of R = 1.35 cm. The two values of the ballast resistance correspond to the two different steady-state discharge currents: ≈0.7 and ≈1.4 mA. In what follows, the two regimes under consideration will be characterized by the corresponding values of the steady-state current. The initial electron density and the population of the metastable levels were assumed to be low, which corresponds to experiments with large time intervals between the discharge pulses. The computation results are presented in Figs. 9–11.

Let us first consider the results obtained with the use of the base model. They are shown by solid curves. Figure 9a shows the time evolution of the discharge current and the reduced electric field in the positive column. It can be seen that, before the steady state is reached, the discharge current passes through a maximum, whose magnitude only slightly exceeds the steady-state current. The nonmonotonic time dependence of the reduced electric field is more pronounced. The reduced field E/N sharply decreases from the initial maximum value to a minimum value, which is almost three times lower than the steady-state reduced field. Thereafter, the reduced field increases and, after a few oscillations, reaches a steady-state level. For both values of the discharge current, the steady-state value of E/N is almost the same, although for $i \approx 1.4$ mA it is a bit lower.

The calculated populations of the lowest metastable level of Ar are shown in Fig. 9b. It can be seen that the

population of the $1s_5$ level increases rapidly from zero to a maximum value and then sharply drops, reaching its steady-state value after a few oscillations. The steady-state populations corresponding to the two values of the discharge currents are close to one another, whereas the maximum population is significantly larger at the higher current. Note also that the populations of the other levels ($1s_4$, $1s_3$, and $1s_2$) are small compared to the population of the $1s_5$ level.

The time evolution of the electron and ion densities is shown in Figs. 10a and 10b, respectively. The electron density behaves similarly to the population of the $1s_5$ level: a rapid increase to the maximum value is followed by a sharp decrease and subsequent damping oscillations. For $i \approx 1.4$ mA, the amplitude of the first maximum in the electron density is much larger than for $i \approx 0.7$ mA (see Fig. 10a). The steady-state values of n_e differ by a factor of 2; i.e., their ratio is equal to the current ratio. The reason for this is that the E/N value is almost the same in both cases. Note that the densities of atomic and molecular ions in both cases are nearly the same (see Fig. 10b).

It follows from Figs. 9 and 10a that the population of the $1s_5$ state reaches its maximum value before the electron density does. The peak in the electron density coincides in time with the dip of the electric field. According to our simulations, the formation of the positive column of an argon glow discharge proceeds as follows: At the initial instant, when the electric field in the plasma is high, the electron density increases sharply due to direct ionization (see Fig. 9a) and the population of the $1s_5$ level grows. As n_e (and, consequently, the discharge current) increases, the electric field in the plasma sharply decreases and direct ionization becomes insignificant as compared to chemionization and stepwise ionization. The rate constant for the excitation of the $1s_5$ level also decreases. Within the framework of our model, the decay rate of this state due to electron mixing and chemionization does not depend on the electric field; therefore, at a certain instant, the production rate of this state becomes equal to the decay rate and the population of the $1s_5$ level reaches its maximum value, which is much larger than the steady-state value. Due to the large concentration of metastable atoms, the rates of both stepwise ionization and chemionization are much higher than the rate of electron loss due to ambipolar diffusion; so, the electron density continuous to grow. Accordingly, the electric field in the plasma decreases. As time elapses, the ionization rate decreases (because of a decrease in the population of the $1s_5$ level) and becomes equal to the rate of ambipolar diffusion. At this instant, the electron density is maximum and the electric field is minimum. Thereafter, the loss of electrons due to ambipolar diffusion dominates over the production of electrons due to ionization and the electron density decreases. This, in turn, leads to an increase in the electric field in the plasma, the maximum electric field being somewhat higher than the steady-state field. Eventually, after a few damping oscillations, the electric field reaches its steady-state value.

The time evolution of the relative contributions from different processes to the rate of electron production and the decay rate of the $1s_5$ level is shown in Fig. 11. It can be seen from Fig. 11a that, when the concentration of metastable atoms is maximum, the contributions from stepwise ionization and chemionization are nearly the same, whereas in the steady-state phase, stepwise ionization prevails. The decay of the $1s_5$ metastable level is mainly caused by electron mixing (see Fig. 11b). Only at the very beginning of the discharge, when the electron density is still relatively low, is the decay of metastable states mainly related to the formation of dimers.

A comparison between the computation and experimental results shows that the model adequately describes the time evolution of the plasma parameters during the formation of the positive column in an argon glow discharge; specifically, it predicts the presence of a peak in the population of the $1s_5$ level and a minimum in the electric field in the initial stage of a discharge. The calculated and measured populations of the $1s_5$ level differ by a factor of less than 2 (cf. Figs. 6, 7, and 9b). Moreover, the calculated steady-state value of E/N agrees well with the measured value (estimated by averaging the data from Figs. 5a and 5e over time). However, in calculations, the period of oscillations of the plasma parameters is shorter and the oscillation amplitude is appreciably smaller than their measured values.

The most drastic difference between the computation and experimental results is that, in calculations, the minimum value of the reduced electric field is much larger than that in the experiment. For example, for $i \approx 0.7$ mA, the calculated minimum value of the reduced field is $(E/N)_{\min} \approx 2.3$ Td, whereas the minimum value of the reduced field estimated from the experimental data is $(E/N)_{\min} \leq 0.5$ Td. Our estimates show that, at $(E/N)_{\min} \approx 2.3$ Td, the emission intensity of the above spectral lines only slightly decreases below its steady-state level. To reduce the calculated value of $(E/N)_{\min}$, it is necessary to increase the maximum electron density. This, in turn, calls for an increase in the population of the $1s_5$ level. In principle, this can be achieved by properly adjusting the cross sections and the rate constants used in our model. For this purpose, test calculations for the case of $i \approx 0.7$ mA were performed in which the cross sections for the excitation of metastable states were increased twofold, the rate constant for electron mixing was decreased fourfold, and the rate of ambipolar diffusion was halved. The relevant computation results are shown in Figs. 9 and 10 by the dashed lines. Let us compare them to the computation results obtained using the base model. It can be seen that the maximum population of the $1s_5$ level increased by ≈15%, the duration of the time interval in which the

population is reduced increased twofold, and the steady-state population decreased by nearly 30%. The maximum electron density increased by ≈28%, whereas the duration of the time interval where n_e is reduced increased twofold. The time evolution of E/N changed most radically. The minimum reduced field $(E/N)_{min}$ decreased by a factor of almost 3.5. The reason for such a significant decrease in $(E/N)_{min}$ is that the electron drift velocity in argon only slightly decreases with decreasing E/N within the range $E/N < 4$ Td. For a fixed current, the 28% increase in the electron density must be balanced by a decrease in the electron drift velocity, which calls for a significant decrease in E/N.

As a whole, the computation results obtained using the test version of the model agree much better with the experiment than those obtained in the base model. The validity of using the test model with modified cross sections and rate constants is questionable, however.

6. CONCLUSIONS

The initial stage of the positive column formation in a low-pressure ($p = 5$ torr) glow discharge in argon has been studied at discharge currents of ~1 mA (specifically, at 0.7 and 1.4 mA). The time evolution of the emission intensities of the spectral lines, the electric field in the discharge plasma, and the population of the lowest metastable state of Ar were measured. It is found that the initial spike in the emission intensity is followed by a 1- to 1.5-ms-long period during which the emission intensity is lower than that in the steady-state phase of the discharge. The duration of this dark phase decreases with increasing discharge current. The time evolution of the electric field also displays a dip in which the reduced electric field E/N is much lower than its steady-state value. At the same time, the population of the $1s_5$ metastable state in the initial stage of the discharge is much higher than that in the steady-state phase.

A kinetic model has been developed to simulate the positive column plasma of a glow discharge in argon by consistently solving the equations for the electron and ion densities and for the populations of the excited states of Ar, the Boltzmann equation for the EEDF, and the equation for the electric circuit. Using this model, we have calculated the time evolution of the plasma parameters (such as the electron density, the reduced electric field, and the population of the metastable levels). The calculated results agree satisfactorily with the experimental data.

Our experimental and theoretical study has shown that the DP effect is related to the production of an excessive amount of metastable Ar atoms at the beginning of the discharge and, consequently, to high rates of stepwise ionization and chemionization. The high ionization rate leads to an increase in the electron density and, accordingly, to a significant decrease in the electric field in the positive column. This, in turn, results in a sharp decrease in the rate constants for the electron-impact excitation of the electronic states of Ar and a decrease in the emission intensity.

It is also shown that quantitative agreement between numerical and experimental results can be achieved by adjusting the cross sections and rate constants incorporated in the model. The validity of such an adjustment is questionable, however.

ACKNOWLEDGMENTS

This study was supported by the Russian Foundation for Basic Research (project no. 03-02-16917) and the "RF Presidential Program for State Support of Leading Scientific Schools" (grant no. 794.2003.2).

REFERENCES

1. Yu. Z. Ionikh, I. N. Kostyukevich, and N. V. Chernysheva, Opt. Spektrosk. **74**, 455 (1993) [Opt. Spectrosc. **74**, 274 (1993)].
2. Yu. Z. Ionikh, Yu. G. Utkin, N. V. Chernysheva, and A. S. Evdokimenko, Fiz. Plazmy **22**, 289 (1996) [Plasma Phys. Rep. **22**, 267 (1996)].
3. R. Kh. Amirov, É. I. Asinovskiĭ, and V. V. Markovets, Teplofiz. Vys. Temp. **19**, 47 (1981).
4. R. Kh. Amirov, É. I. Asinovskiĭ, and V. V. Markovets, Fiz. Plazmy **27**, 450 (2001) [Plasma Phys. Rep. **27**, 424 (2001)].
5. K. Tachibana, Phys. Rev. A **34**, 1007 (1986).
6. M. Hayashi, Report No. IPPJ-AM-19 (Institute of Plasma Physics, Nagoya University, Nagoya, 1981).
7. D. Rapp and P. Englander-Golden, J. Chem. Phys. **43**, 1464 (1965).
8. M. A. Khakoo, P. Vandeventer, J. G. Childers, *et al.*, J. Phys. B **37**, 247 (2004).
9. A. Chutjian and D. C. Cartwright, Phys. Rev. A **23**, 2178 (1981).
10. V. A. Rozhanskiĭ and L. D. Tsendin, *Collisional Processes in Partially Ionized Plasma* (Énergoatomizdat, Moscow, 1988) [in Russian].
11. Yu. P. Raizer, *Gas Discharge Physics* (Nauka, Moscow, 1987; Springer-Verlag, Berlin, 1991).
12. *Tables of Physical Quantities*, Ed. by I. K. Kikoin (Atomizdat, Moscow, 1976) [in Russian].
13. W. Schottky, Phys. Z. **25**, 635 (1924).
14. F. W. Crawford, J. Appl. Phys. **51**, 1422 (1980).
15. G. L. Rogoff, J. Appl. Phys. **52**, 6601 (1981).
16. C. M. Ferreira and J. Loureiro, J. Appl. Phys. **57**, 82 (1985).
17. A. J. Dixon, M. F. A. Harrison, and A. C. H. Smith, *VIII International Conference on the Physics of Electronic and Atomic Collisions, Belgrade, 1973*, Abstracts of Papers, Vol. 1, p. 405.
18. D. Ton-That and M. R. Flannery, Phys. Rev. A **15**, 517 (1977).
19. H. A. Hyman, Phys. Rev. A **20**, 855 (1979).

20. N. B. Kolokolov, in *Plasma Chemistry*, Ed. by B. M. Smirnov (Énergoatomizdat, Moscow, 1985), Vol. 13 [in Russian].
21. N. B. Kolokolov and A. B. Blagoev, Usp. Fiz. Nauk **163** (3), 55 (1993) [Phys. Usp. **36**, 152 (1993)].
22. V. B. Borisov, V. S. Egorov, and N. A. Ashurbekov, *IV All-Union Conference on Physics of Low-Temperature Plasma, Leningrad, 1983*, Abstracts of Papers, p. 20.
23. Z. Donko, N. Sadeghi, N. Baguer, and A. Bogaerts, in *Proceedings of the 17th European Conference on Atomic and Molecular Physics of Ionized Gases, Constanta, 2004*, p. 161.
24. L. I. Virin, G. V. Dzhagatspanyan, R. V. Karachevtsev, *et al.*, *Ion–Molecule Reactions in Gases* (Nauka, Moscow, 1979) [in Russian].
25. M. A. Biondi, in *Plinciples of Laser Plasmas*, Ed. by G. Bekefi (Wiley, New York, 1976; Énergoizdat, Moscow, 1982).
26. K. Bartschat and V. Zeman, Phys. Rev. A **59**, R2552 (1999).
27. A. Dasgupta, K. Bartschat, D. Vaid, *et al.*, Phys. Rev. A **65**, 042724 (2002).
28. V. M. Donnelly, J. Phys. D **37**, R217 (2004).
29. V. A. Ivanov and I. V. Makasyuk, Opt. Spektrosk. **69**, 514 (1990).
30. A. Dasgupta, M. Blaha, and J. L. Giuliani, Phys. Rev. A **61**, 012703 (2000).
31. A. Dasgupta, M. Blaha, and J. L. Giuliani, Phys. Rev. A **65**, 039905(E) (2002).
32. C. M. Maloney, J. L. Peacher, K. Bartschat, and D. H. Madison, Phys. Rev. A **61**, 022701 (2000).
33. B. J. Boffard, G. A. Piech, M. F. Gehrke, *et al.*, Phys. Rev. A **59**, 2749 (1999).
34. L. M. Biberman, V. S. Vorob'ev, and I. T. Yakubov, *Kinetics of Nonequilibrium Low-Temperature Plasmas* (Nauka, Moscow, 1982; Consultants Bureau, New York, 1987).
35. A. A. Radtsig and B. M. Smirnov, *Reference Data on Atoms, Molecules, and Ions* (Énergoatomizdat, Moscow, 1986; Springer-Verlag, Berlin, 1985).
36. C. Brow, in *Excimer Lasers*, Ed. by C. K. Rhodes (Springer-Verlag, New York, 1979; Mir, Moscow, 1981).
37. N. A. Dyatko, I. V. Kochetov, A. P. Napartovich, and M. D. Taran, Preprint No. 3842/12 (Kurchatov Institute of Atomic Energy, Moscow, 1983).
38. E. A. Bogdanov, A. A. Kudryavtsev, L. D. Tsendin, *et al.*, Zh. Tekh. Fiz. **74** (6), 44 (2004) [Tech. Phys. **49**, 698 (2004)].

Translated by N.N. Ustinovskiĭ